INFECTION AND IMMUNITY, July 1999, p. 3571–3579 Vol. 67, No. 7
0019-9567/99/$04.00+0

Fatal Granuloma Necrosis without Exacerbated Mycobacterial Growth in Tumor Necrosis Factor Receptor p55 Gene-Deficient Mice Intravenously Infected with *Mycobacterium avium*

STEFAN EHLERS,[1]* JOCHEN BENINI,[1] STEFANIE KUTSCH,[1] ROBERT ENDRES,[2] ERNST T. RIETSCHEL,[1] AND KLAUS PFEFFER[2]

Division of Molecular Infection Biology, Research Center Borstel, D-23845 Borstel,[1] and Institute of Medical Microbiology, Immunology and Hygiene, Technical University, D-81675 Munich,[2] Germany

Received 19 October 1998/Returned for modification 25 January 1999/Accepted 14 April 1999

The pathogenesis of mycobacterial infections is associated with the formation of granulomas in which both antibacterial protection and tissue damage take place concomitantly. We used murine *Mycobacterium avium* infection to compare the development of granulomatous lesions in intravenously infected tumor necrosis factor receptor p55 (TNFRp55) gene-deficient ($p55^{-/-}$) mice to the development of granulomatous lesions in *M. avium*-infected syngeneic C57BL/6 ($p55^{+/+}$) mice. Up to 5 weeks after infection with either the highly virulent *M. avium* strain TMC724 or the intermediately virulent *M. avium* strain SE01, bacterial counts in the liver, spleen, and lung of $p55^{-/-}$ mice were identical to or lower than those in infected $p55^{+/+}$ mice. However, the formation of mononuclear cell foci in the liver was delayed by approximately 2 to 3 weeks in $p55^{-/-}$ mice compared to the results obtained for infected $p55^{+/+}$ mice. Despite comparable bacterial loads, granulomas in $p55^{-/-}$ mice underwent progressive necrosis, causing damage to the surrounding liver tissue. The appearance of necrotizing granulomas was associated with the death of all infected $p55^{-/-}$ mice, regardless of the virulence of the *M. avium* strain used for infection. Granulomatous lesions in the liver contained three times as many $CD3^+$ cells in $p55^{-/-}$ mice yet appeared more diffuse than in $p55^{+/+}$ mice. Semiquantitative reverse transcription-PCR studies revealed that prior to mouse death, interleukin-12 (IL-12) and gamma interferon mRNA levels were up regulated in the livers of infected $p55^{-/-}$ mice, while mRNA levels for tumor necrosis factor, the inducible isoform of nitric-oxide synthase (iNOS), and IL-10 were similar to those found in infected $p55^{+/+}$ mice. In response to persistent mycobacterial infection, the absence of TNFRp55 causes the disregulation of T-cell–macrophage interactions and results in fatal granuloma necrosis even when adequate antibacterial functions are maintained.

Granulomas are focal mononuclear cell infiltrations that appear in response to chronic inflammatory stimuli and are therefore a hallmark of mycobacterial infections. Granulomas are an essential component of a coordinated antimycobacterial defense, because it is within granulomas that T-cell–macrophage cooperation can take place, allowing the macrophage to display effective bacteriostatic or bacteriocidal activities (9, 24). On the other hand, granulomas displace and destroy adjacent tissues, leading to inflammation-dependent organ damage or failure (9, 23).

The inflammatory and protective components of the host immune response against mycobacteria coincide temporally and may be mediated by the same molecules. A case in point, tumor necrosis factor (TNF) has been shown with in vitro and in vivo studies to induce antibacterial mechanisms in macrophages against *Mycobacterium tuberculosis* and *Mycobacterium avium* (2, 14, 17). In addition, TNF plays a pivotal role in mononuclear cell recruitment, because a polyclonal antiserum against TNF reduced granuloma induction and accelerated granuloma resolution in mice infected with *Mycobacterium bovis* BCG (25). Similarly, in SCID mice infected with *M. avium*, T-cell-independent granuloma formation was completely abrogated by treatment with a monoclonal antibody against TNF (38).

When mice genetically deficient for the major signalling component of the TNF receptor p55 (TNFRp55) ($p55^{-/-}$ mice) were infected with live *M. bovis* BCG or killed *Corynebacterium parvum*, they developed fewer and smaller granulomas than wild-type control mice (37). However, when *M. tuberculosis* was used to infect $p55^{-/-}$ mice, granuloma formation was found to proceed in an almost unaltered fashion (17). In the latter experiments, and in studies using transgenic mice expressing soluble TNFRp55 fusion protein, which effectively neutralizes the activity of soluble TNF, mutant mice exhibited greatly increased bacterial organ loads with concomitant tissue necrosis and prematurely succumbed to infection (17, 18). With these models, it has been impossible to distinguish between direct mycobacteriostatic effects and the granulomagenic properties of TNF, and the effects of the lack of TNFRp55-mediated signalling on granuloma maintenance in chronic mycobacterial persistence could not be studied.

M. avium is the cause of the most prevalent opportunistic infection among AIDS patients (21). Disseminated *M. avium* infection in these patients leads to hepatosplenomegaly with variable granuloma formation, anemia, fever, and weight loss (22, 26). Studies using chemotherapy prophylaxes have shown that quality of life and life expectancy are both significantly reduced by *M. avium* infection in these patients (20, 22).

In mice, all strains of *M. avium* are less virulent than *M. tuberculosis*, and murine *M. avium* infection is more chronic by nature (6, 33). In addition, mice tolerate much higher bacterial numbers (up to 10^{10} CFU) in organs during *M. avium* infection than during *M. tuberculosis* infection (1, 19). *M. avium* infec-

* Corresponding author. Mailing address: Division of Molecular Infection Biology, Research Center Borstel, Parkallee 22, D-23845 Borstel, Germany. Phone: 49-4537-188481. Fax: 49-4537-188686. E-mail: sehlers@fz-borstel.de.

tion therefore allows for a more detailed kinetic analysis of granuloma induction and maintenance than infections with highly virulent organisms like *M. tuberculosis* or *Listeria monocytogenes*, which may cause rapid tissue destruction. In addition, in vivo studies using neutralizing antibodies against TNF demonstrated only a marginal, if any, effect on *M. avium* replication during the early phase of infection (1). We therefore used *M. avium* infection to examine the contribution of TNFRp55-mediated signals in maintaining long-term granuloma integrity in response to a persistent replicating stimulus of low intrinsic toxicity.

MATERIALS AND METHODS

Mice. TNFRp55$^{-/-}$ mice were obtained as described (34). The mice used in the studies presented here are fifth generation backcrosses onto a C57BL/6J strain. The murine TNFRp55 gene (*Tnfrsfla*) maps to mouse chromosome 6 at 57.10 centimorgans (cM) (4, 32). Neighboring genes that are linked within 0.5 cM upstream and downstream encode Bphs (*Bordetella pertussis*-induced histamine sensitization), CD9, lymphotoxin-β receptor, nucleolar protein 1, CD27, and Idd19 (insulin-dependent diabetes mellitus 19). No information about allelic variants within these loci between 129/Sv and C57BL/6 has been reported so far. The p55$^{-/-}$ and syngeneic C57BL/6 p55$^{+/+}$ mice were raised in the animal breeding facilities of the GSF-National Research Center for Environment and Health (Oberschleissheim, Germany) and (for repeat experiments) by Charles River Wiga (Sulzfeld, Germany). For the course of *M. avium* infection, age- and sex-matched groups of p55$^{+/+}$ and p55$^{-/-}$ mice were housed in isolator cages under barrier conditions at the Institute for Medical Microbiology, Munich, or in the animal facilities at the Borstel Research Center.

Bacteria. *M. avium* TMC724 (originally obtained from F. Collins, Trudeau Institute, Saranac Lake, N.Y.) and *M. avium* SE01 (an isolate from the blood culture of an AIDS patient) were passaged twice in C57BL/6 mice and cultured in Middlebrook 7H9 (Difco, Detroit, Mich.) medium supplemented with OADC (oleic acid, albumin, dextrose, catalase; Becton Dickinson, Heidelberg, Germany) to mid-logarithmic phase. Aliquots of the cultured organisms were frozen at −70°C until needed. An inoculum of bacteria was prepared by thawing an aliquot and diluting it in phosphate-buffered saline (PBS). Mice were infected intravenously via a lateral tail vein with indicated inocula in 0.2 ml of PBS. Mice were anesthetized and killed at indicated time points during the course of infection. Organs were removed aseptically and homogenized in 10 ml of distilled water to determine bacterial loads by plating serial 10-fold dilutions of whole-organ homogenates on nutrient Middlebrook 7H10 agar (Difco) supplemented with OADC. Bacterial colony numbers were determined after 14 to 21 days of incubation at 37°C in humidified air. The natural course of infection and the kinetics of granuloma formation in mice infected with these strains were previously described (19).

Histology. One cranial and one caudal liver lobe per mouse were fixed in 4% formaline-PBS, set in paraffin blocks, sectioned (2- to 3-μm sections), and stained using hematoxylin and eosin (HE), or, for easier visualization of apopotic cells, with toluidine blue. Granuloma numbers were determined by counting focal mononuclear infiltrations in five nonsequential sections per animal (four mice per group) in a superimposed 0.25-cm^2 grid. For the purpose of quantitation, a granuloma was defined as the focal accumulation of more than nine mononuclear cells. Data represent the means of 20 determinations ± standard deviations (SD).

Immunohistology. Tissue sections were deparaffinated and placed in 10 mM sodium citrate buffer (pH 6) and pressure-cooked for exactly 1 min (5). After blocking for 20 min in 1% H_2O_2 solution, slides were incubated with appropriately diluted polyclonal rabbit anti-mouse-isoform of nitric-oxide synthase (iNOS) (Genzyme-Virotech, Rüsselsheim, Germany) in Tris-buffered saline–10% fetal calf serum for 30 min in a humid chamber. Appropriately diluted goat-anti-rabbit immunoglobulin G (IgG) peroxidase (Dianova, Hamburg, Germany) was used as a bridging antibody and diluted rabbit anti-goat IgG peroxidase (Dianova) was used as a tertiary antibody in sequential incubations of 30 min each. For the detection of CD3$^+$ cells, a rat anti-mammalian CD3 monoclonal antibody (clone CD3-1C; Biotrend, Cologne, Germany) was used as a primary antibody, diluted rabbit anti-rat IgG (Dianova) as a secondary antibody, and goat anti-rabbit IgG peroxidase as a tertiary antibody. Development was performed with 3-3′-diaminobenzidine (Sigma, Deisenhofen, Germany) and urea superoxide (Sigma), and hemalum was used to counterstain the slides.

RT-PCR. A detailed protocol of the procedure employed for semiquantitative reverse transcription (RT)-PCR has been published elsewhere (13, 19). Briefly, weighed liver samples (approximately 150 mg each) were homogenized in 5 ml of 4 M guanidinium-isothiocynanate buffer, diluted to obtain equalized amounts of liver in buffer, and after acid phenol extraction of total RNA, cDNA was obtained by using Moloney murine leukemia virus-RT (Gibco-BRL, Eggenstein, Germany) and deoxyribosylthymdine (12- to 18-mer; Sigma) as a primer. After amplification (denaturation at 94°C for 30 s, annealing at 60°C for 30 s, and extension at 72°C for 30 s) and electrophoresis on a 2% agarose gel, amplicons were blotted onto a nylon membrane (Hybond N+; Amersham-Pharmacia, Freiburg, Germany), and hybridization was performed at 42°C with specific internal oligonucleotide probes (followed by two washes at room temperature) and 45°C under increasingly stringent salt conditions. Chemiluminescent labelling and detection of hybridized oligonucleotides were performed by using the Amersham ECL kit and autoradiography for approximately 90 min on Hyperfilm-ECL (Amersham-Pharmacia). The following specific cytokine primers and probes and PCR cycle numbers were used: β2-microglobulin (14 cycles), sense 5′-TGACCGGCTTGTATGCTATC-3′ and antisense 5′-CAGTGTGAGCCAG GATATAG-3′ with probe 5′-GAAGCCGAACATACTGAACTGCTAC-3′; interleukin-10 (IL-10) (26 cycles), sense 5′-CGGGAAGACAATAACTG-3′ and antisense 5′-CATTTCCGATAAGGCTTGG-3′ with probe 5′-GGACTGGCTT CAGCCAGGTGAAGAC-3′; IL-12 p40 (26 cycles), sense 5′-CGTGCTCATG GCTGGTGCAAAG-3′ and antisense 5′-CTTCATCTGCAAGTTCTTGGG C-3′ with probe 5′-TCTGTCTGCAGAGAAGGTCACA-3′; gamma interferon (IFN-γ) (24 cycles), sense 5′-AACGCTACACACTGCATCTTGG-3′ and antisense 5′-GACTTCAAAGAGTCTGAGG-3′ with probe 5′-GGAGGAACTGG CAAAAGGA-3′; TNF (22 cycles), sense 5′-GATCTCAAAGACAACCAACT AGTG-3′ and antisense 5′-CTCCAGCTGGAAGACTCCTCCCAG-3′ with probe 5′-CCCGACTACGTGCTCCTCACC-3′; and iNOS (26 cycles), sense 5′-CTGGAGGAGCTCCTGCCTCATG-3′ and antisense 5′-GCAGCATCCCCTC TGATGGTG-3′ with probe 5′-CTGGATGAGCTCATCTTTGCC-3′.

PCR conditions were optimized to ensure that the PCR was performed in the exponential phase. Serial twofold dilutions of positive-control cDNA were included in each reaction and subsequent hybridization to confirm that the PCR had not reached a plateau. This titration was used as a calibrated, semiquantitative scale for comparison of amplicon intensities from different experimental samples. As a control for calibrating an equivalent amount of input cDNA, amplification for β2-microglobulin was performed, and all samples were equalized (if necessary) for β2-microglobulin cDNA content prior to analysis of cytokine cDNA. Quantitation was performed after scanning hyperfilm radiographs with a Studiostar scanner (Agfa, Cologne, Germany), and the number of black pixels over background film was measured by using Photoshop software (Adobe, Edinburgh, United Kingdom) in a preset frame of 3,750 total pixels. Statistical analysis was carried out with pixel values obtained from four mice per experimental group. Fold increase over background was calculated from the titration of the standard cDNA, assigning an arbitrary value of 1 to the titer with background pixel levels. Fold differences between experimental groups were calculated by comparing fold increases of p55$^{+/+}$ mice to levels of p55$^{-/-}$ mice infected with the same strain.

Cytokine ELISAs, nitrite-nitrate measurements, and determination of liver enzyme levels. Roughly similar-sized pieces of spleen were weighed (each piece was approximately 300 to 400 mg, except for controls, which weighed 70 to 80 mg) and homogenized in 2 ml of PBS containing 10 μg of chymostatin per ml, 5 μg of leupeptin per ml, and 10 μg of aprotinin (Boehringer, Mannheim, Germany) per ml. Homogenates were diluted with PBS to equalize the concentrations of spleen in the samples. Samples were centrifuged at 6,500 rpm for 15 min in an Eppendorf microcentrifuge, after which the supernatant was stored at −70°C. Plasma was obtained after centrifugation of heparinized blood drawn from the inferior vena cava of anesthetized mice and stored at −70°C until further use. Enzyme-linked immunosorbent assay (ELISA) measurements of TNF and IFN-γ levels in the plasma and spleen homogenates were carried out as stipulated by the manufacturer (Genzyme-Virotech, Rüsselsheim, Germany), and concentrations were calculated per input organ weight. As an indicator of nitric oxide production, the concentrations of the final reaction products nitrate and nitrite were determined in the plasma by a colorimetric method (Boehringer), appropriately scaled down to microtiter plate format to accommodate 50-μl samples. For use in this assay, plasma samples were diluted twofold, added to a microconcentrator (Amicon, Beverly, Mass.) (cutoff, 10,000 Da), and centrifuged at 6,000 rpm for 15 min followed by 8,000 rpm for 30 min in an Eppendorf microcentrifuge. Levels of aspartate aminotransferase (ASAT), alanine aminotransferase (ALAT), and lactatedehydrogenase (LDH) were measured in the plasma of mice by using standard procedures and an automated sample analyzer in the laboratory of clinical biochemistry of the Borstel Clinical Center.

Statistics. Quantifiable data are expressed as the means of individual determinations ± SD. Statistical analysis was performed by using Student's *t* test or Welch analysis of variance in cases of unequal variances.

RESULTS

Course of *M. avium* infection in p55$^{+/+}$ and p55$^{-/-}$ mice. During the first 5 weeks following intravenous infection with either 10^5 or 10^6 CFU of the virulent TMC724 strain, the bacterial counts in the liver and lungs of p55$^{+/+}$ and p55$^{-/-}$ mice were almost identical (Fig. 1A and E). Infection with either 1×10^5 or 8×10^6 CFU of the less-virulent SE01 strain resulted in similar growth curves in the liver and lungs of p55$^{+/+}$ and p55$^{-/-}$ mice (Fig. 1B and F). The plateau of

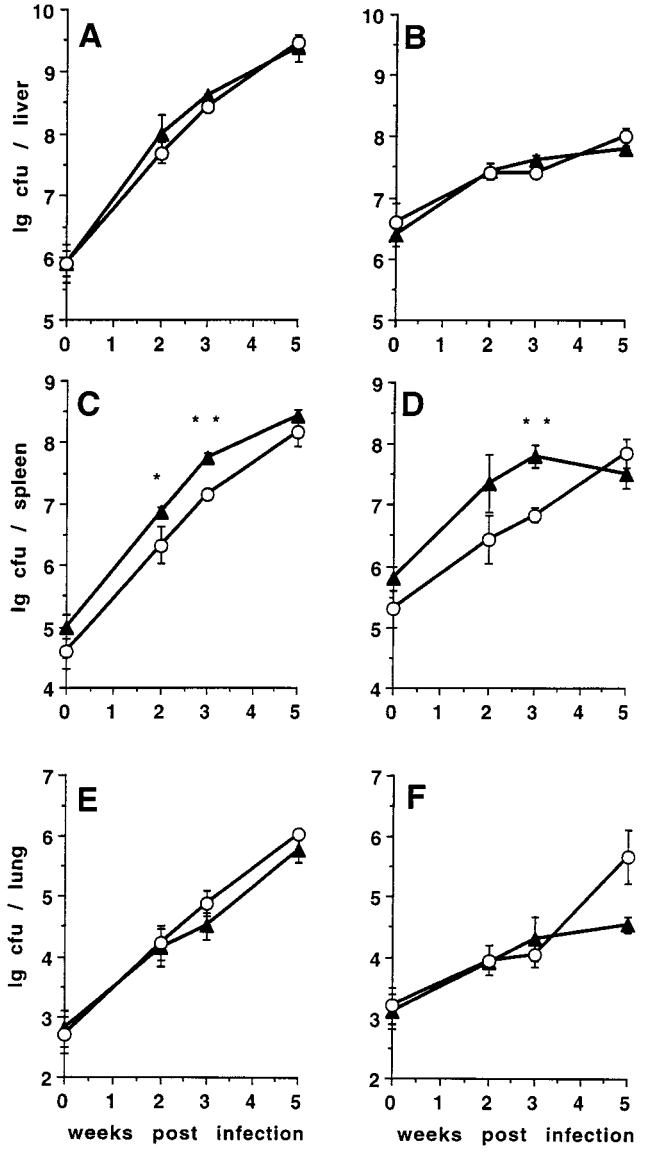

FIG. 1. Course of *M. avium* infection in $p55^{+/+}$ and $p55^{-/-}$ C57BL/6 mice. Mice were intravenously infected with either 1×10^6 CFU of *M. avium* TMC724 (A, C, and E) or 8×10^6 CFU of *M. avium* SE01 (B, D, and F), and bacterial counts were determined in the liver (A and B), spleen (C and D), and lungs (E and F) at indicated time points. Each point reflects the means and SD (error bars) of four mice per group. Triangles, $p55^{+/+}$ mice; circles, $p55^{-/-}$ mice; *, $P < 0.05$; **, $P < 0.005$.

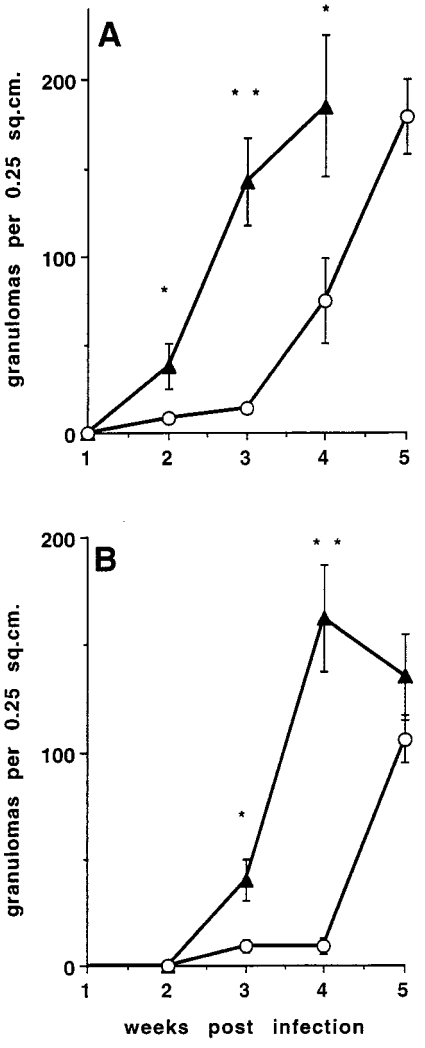

FIG. 2. Granuloma formation in *M. avium*-infected $p55^{+/+}$ and $p55^{-/-}$ C57BL/6 mice. Mice were intravenously infected with 10^5 CFU of either *M. avium* TMC724 (A) or *M. avium* SE01 (B). At indicated time points, the number of granulomas in an area of 0.25 cm^2 were determined on nonsequential sections of HE-stained liver tissue. Each point reflects the means and SD (error bars) of 20 determinations (five sections per mouse, four mice per group). Triangles, $p55^{+/+}$ mice; circles, $p55^{-/-}$ mice; *, $P < 0.005$; **, $P < 0.0001$.

bacterial growth reached after 2 weeks of infection with this strain in the livers of $p55^{+/+}$ mice was also evident in $p55^{-/-}$ mice, showing early mycobacteriostatic effector mechanisms to be intact in these mice. In one of three experiments, bacterial counts in the lungs of $p55^{-/-}$ mice infected with SE01 were significantly higher than in $p55^{+/+}$ mice at 5 weeks postinfection ($P < 0.05$). Following infection with either strain, $p55^{-/-}$ mice always had significantly lower bacterial loads in their spleen at early time points of infection ($P < 0.01$) (Fig. 1C and D). This could be attributed to the smaller size of the spleens of $p55^{-/-}$ mice, as bacterial loads were identical between $p55^{+/+}$ and $p55^{-/-}$ mice when CFU counts were expressed as the log of CFU per gram of tissue (data not shown).

Kinetics and morphology of granuloma formation in response to *M. avium* infection in $p55^{+/+}$ and $p55^{-/-}$ mice. During early infection of $p55^{-/-}$ mice with 10^5 or 10^6 CFU of *M. avium* (TMC724 or SE01) there were numerous Kupffer cells filled with acid-fast material that were not surrounded by inflammatory cells, while this was very rarely observed in control infected mice. In $p55^{-/-}$ mice, these foci of infection without an inflammatory response persisted throughout the course of infection, while $p55^{+/+}$ mice increasingly developed inflammatory cell infiltrations.

Following infection with the lower dose, granuloma initiation and splenomegaly in $p55^{-/-}$ mice were delayed by approximately 2 weeks in mice infected with TMC724 and by 3 weeks in mice infected with SE01 compared to $p55^{+/+}$ mice (Fig. 2). Mononuclear cell infiltrations were more diffuse in $p55^{-/-}$ mice and lacked the appearance of mature granulomas because they contained fewer macrophages showing the typical light-microscopic signs of epithelioid differentiation (elonga-

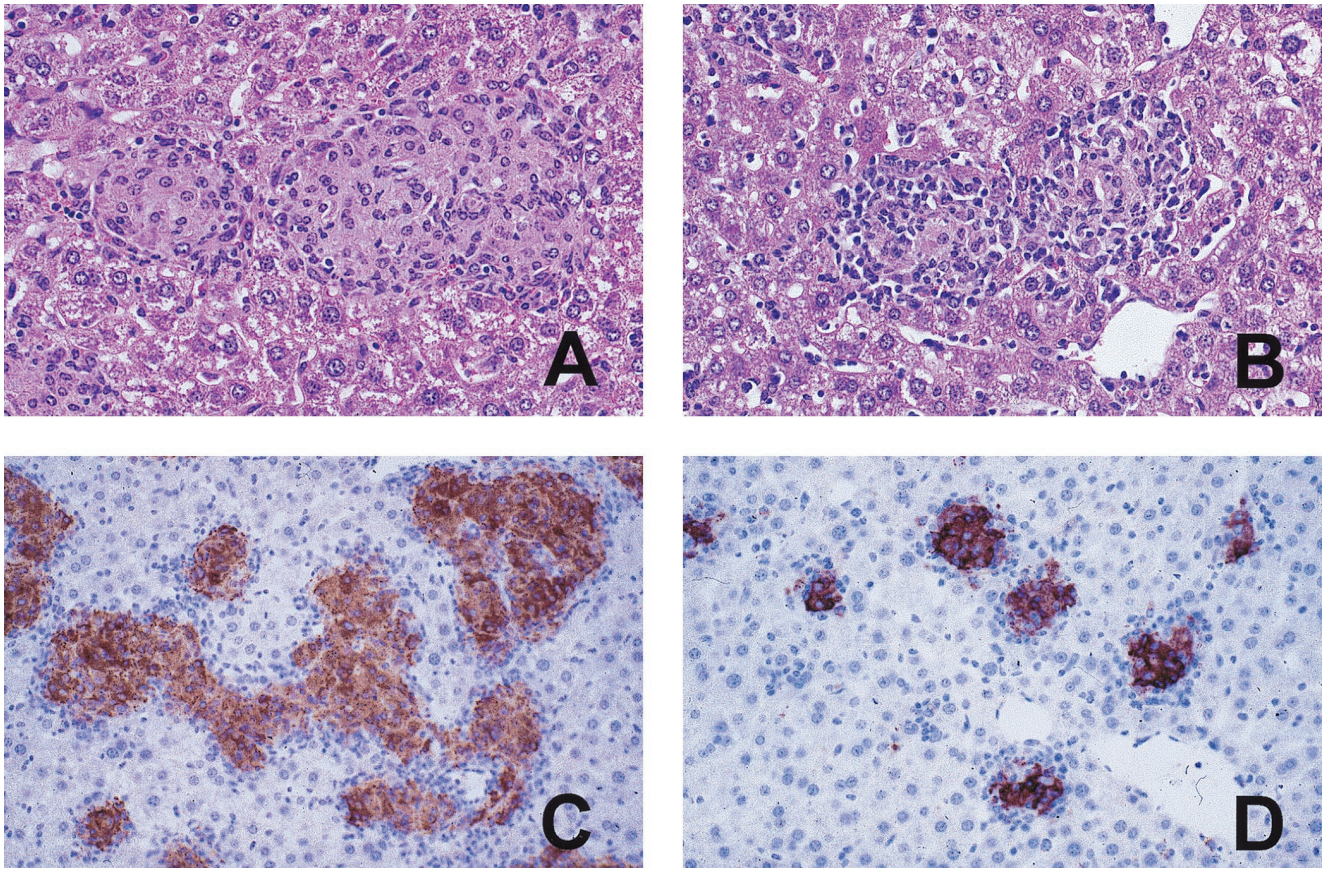

FIG. 3. Granuloma morphology in *M. avium*-infected $p55^{+/+}$ and $p55^{-/-}$ mice. Mice were intravenously infected with 10^6 CFU of *M. avium* TMC724 and sacrificed 5 weeks postinfection. Liver sections were stained with HE (A and B) or with a rabbit anti-iNOS antiserum (immunoperoxidase stain; C and D). (A) Large epithelioid granulomas in a $p55^{+/+}$ mouse (magnification, ×200). (B) Smaller, less well organized granulomas in a $p55^{-/-}$ mouse (×200). (C) Large, confluent, iNOS-positive granulomas in a $p55^{+/+}$ mouse (×64). (D) Small, circumscript, iNOS-positive granulomas in a $p55^{-/-}$ mouse (×64).

tion of nuclei and enlargement of cytoplasm) (Fig. 3A and B). Immunohistological staining of material reactive with a specific rabbit polyclonal anti-iNOS antiserum within the granulomas was equally intense in $p55^{-/-}$ and $p55^{+/+}$ mice (Fig. 3C and D).

When 10- to 50-fold higher inocula of *M. avium* TMC724 or SE01, respectively, were used for infection, granuloma formation and splenomegaly in $p55^{-/-}$ mice were accelerated compared to the lower-dose infection but still proceeded in a delayed and less well organized fashion compared to high-dose infection in $p55^{+/+}$ mice.

Loss of granuloma integrity during chronic *M. avium* infection in $p55^{-/-}$ mice. Within 6 to 8 weeks of receiving 10^5 CFU of TMC724 or SE01, or 3 to 4 weeks after receiving 1×10^6 CFU of TMC724 or 8×10^6 CFU of SE01, $p55^{-/-}$ mice began to look sick, and all *M. avium*-infected gene-deficient mice subsequently died within approximately 10 days. Autopsies performed within this time frame revealed that cellular integrity was severely impaired in all granulomas of infected $p55^{-/-}$ mice, while infected $p55^{+/+}$ mice showed typical, well-differentiated monocytic lesions and control uninfected $p55^{-/-}$ mice had normal liver and spleen histologies at that time. Prior to 5 weeks postinfection, infected $p55^{-/-}$ mice showed no evidence of granuloma necrosis. Early disintegrating granulomas in $p55^{-/-}$ mice in the 6th week of infection showed typical signs of apoptosis, like chromatin condensation and the appearance of pyknotic nuclei, although this was a rare occurrence in intact granulomas of $p55^{+/+}$ mice (Fig. 4A and B). Ziehl-Neelsen staining revealed that all of these lesions in $p55^{-/-}$ mice contained extracellular acid-fast bacilli, showing that these lesions originated from lysed macrophages in granulomatous foci of infection, while in $p55^{+/+}$ mice, acid-fast mycobacteria were always found within macrophages (data not shown).

Loss of macrophage integrity in $p55^{-/-}$ mice was followed by extensive granuloma necrosis in the liver and damage to adjacent liver tissue regardless of the isolate used for infection (Fig. 5B and C). Granuloma necrosis and hepatocyte damage appeared to be progressive, since mice randomly selected for histology after the 5th week of infection showed necrotizing granulomas at different stages of development. In particular, mice that appeared healthy had only a few necrotic granulomas, while mice that appeared very sick showed abundant granuloma necrosis and widespread hepatocyte damage.

All infected, moribund $p55^{-/-}$ mice had significantly increased serum levels of liver enzymes compared to infected $p55^{+/+}$ mice (levels in $p55^{+/+}$ mice were [ASAT] 72 ± 28 U/ml, [ALAT] 55 ± 19 U/ml, and [LDH] 222 ± 67 U/ml; levels in $p55^{-/-}$ mice were [ASAT] 983 ± 340 U/ml, [ALAT] 381 ± 144 U/ml, and [LDH] 7,442 ± 2,413 U/ml; and levels in uninfected $p55^{-/-}$ mice were [ASAT] 15 ± 5 U/ml, [ALAT] 5 ± 4 U/ml, [LDH] 70 ± 20 U/ml). In two repeat experiments performed with 5×10^6 to 8×10^6 CFU of the less-virulent SE01 strain, 20 of 20 $p55^{-/-}$ mice died between 5 and 6 weeks after infection, showing signs of granuloma necrosis, while all syn-

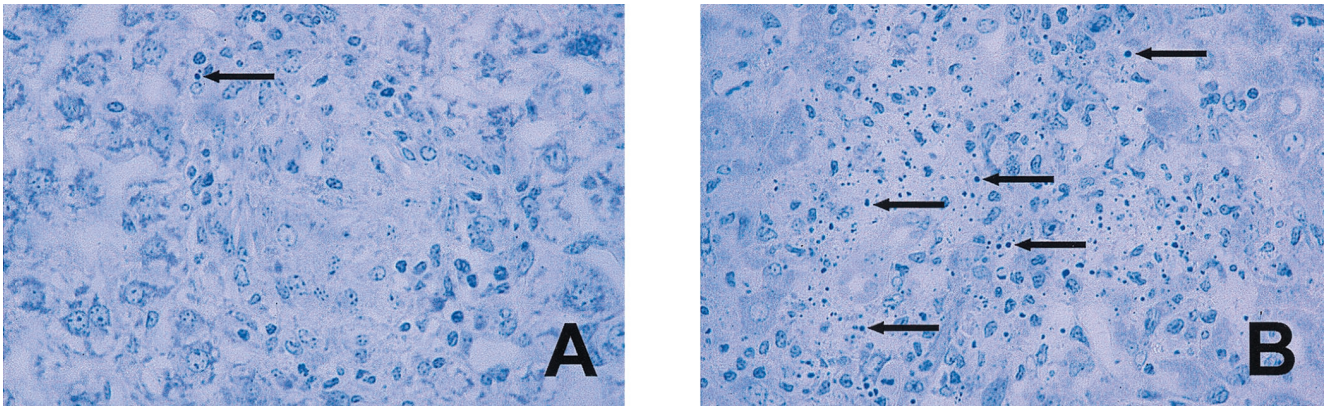

FIG. 4. Apoptotic cells within granulomas of *M. avium*-infected $p55^{-/-}$ mice. Mice were intravenously infected with 10^6 CFU of *M. avium* TMC724 and sacrificed 5 to 6 weeks postinfection for histological analysis of the liver. (A) Well-structured granuloma with epithelioid macrophages and a rare apoptotic cell in a $p55^{+/+}$ mouse; (B) apoptotic cells and multiple pyknotic nuclei in early disintegrating granuloma of a $p55^{-/-}$ mouse (toluidine blue; magnification, ×128). Arrows, apoptotic cells.

geneic $p55^{+/+}$ infected mice were healthy for the length of the experiment (4 months) and showed no structural impairment of granulomas (19). Moribund infected $p55^{-/-}$ mice also had significantly higher bacterial counts in the kidney, brain, and blood, but there was no evidence of necrosis in lungs, spleens, kidneys, or brains at the time of death of these mice.

Evidence for immune disregulation in $p55^{-/-}$ mice infected with *M. avium*. In an attempt to elucidate what precipitated the death of infected $p55^{-/-}$ mice, we investigated the cellular composition and mRNA expression of regulatory cytokines at the site of infection. Immunohistology of the liver at 5 weeks postinfection revealed that there were approximately three times the number of $CD3^+$ cells present in the inflammatory lesions of TMC724-infected $p55^{-/-}$ mice compared to the number present in $p55^{+/+}$ mice (120 ± 21 versus 44 ± 6 granuloma-associated $CD3^+$ cells per 400× microscopic field) (an example is shown in Fig. 6). Similar changes in $CD3^+$ cell numbers were found in SE01-infected $p55^{-/-}$ mice. The increase in $CD3^+$ cells was accounted for by an increase in both the $CD4^+$ and the $CD8^+$ subpopulations of T cells (data not shown). In $p55^{+/+}$ mice, $CD3^+$ cells were always confined to granulomas, whereas they were also found scattered throughout the liver sinusoids in $p55^{-/-}$ mice. To rule out the possibility that there might be a kinetic, rather than an absolute, difference in the number of $CD3^+$ cells recruited to granulomatous lesions in $p55^{-/-}$ versus $p55^{+/+}$ mice, granulomas were also evaluated for their $CD3^+$ cell content at 3 weeks postinfection with *M. avium*. Although incipient granulomas of $p55^{-/-}$ mice were rather small when compared to established lesions in $p55^{+/+}$ mice at this time point, similar numbers of $CD3^+$ cells were detected (Fig. 6A and B). At no time did $p55^{+/+}$ mouse lesions display the high numbers of $CD3^+$ cells evident in $p55^{-/-}$ mouse lesions at 5 weeks postinfection.

Semiquantitative RT-PCR measurements conducted at 3

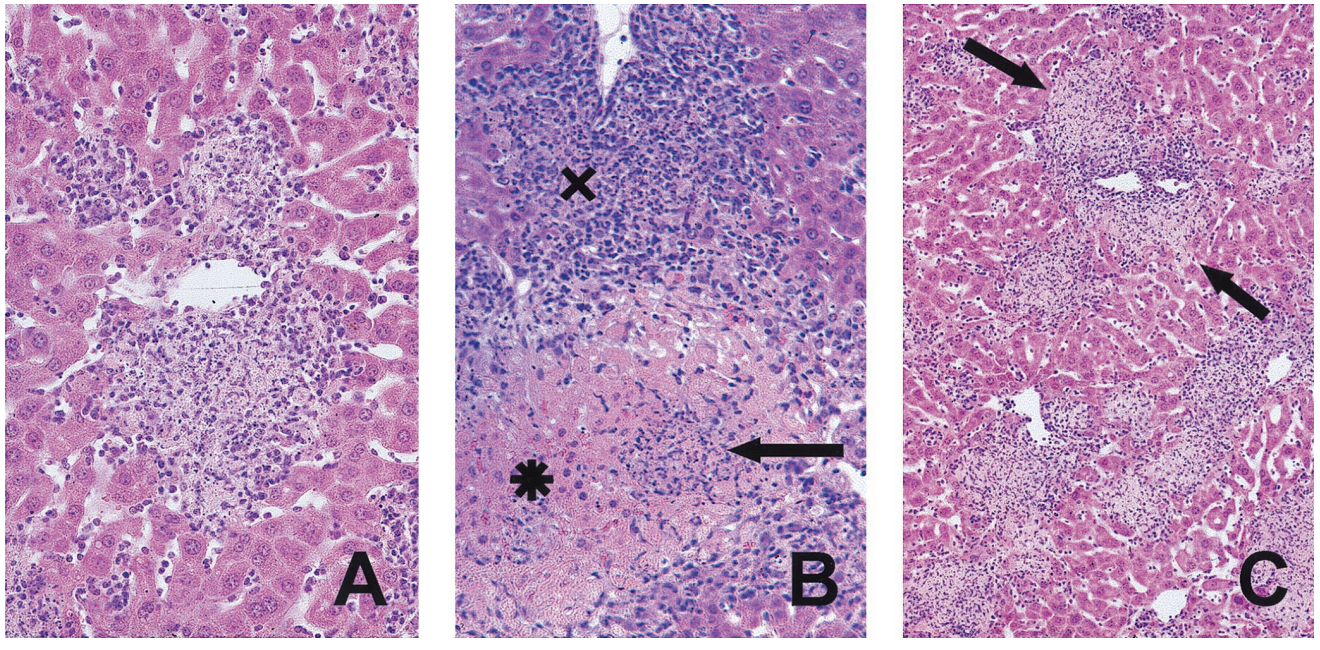

FIG. 5. Granuloma necrosis in *M. avium*-infected $p55^{-/-}$ mice. Mice were intravenously infected with 10^6 CFU of *M. avium* TMC724 and sacrificed 5 to 6 weeks postinfection for histological analysis of the liver. (A) Necrotizing granuloma (HE; magnification, ×200); (B) early necrotizing granuloma (X) and completely disintegrated granuloma (arrow) with leakage into adjacent liver tissue (✶) (HE; magnification, ×128); (C) low-power view of multiple foci of granuloma necrosis with incipient damage (arrows) to surrounding liver tissue (HE; magnification, ×64).

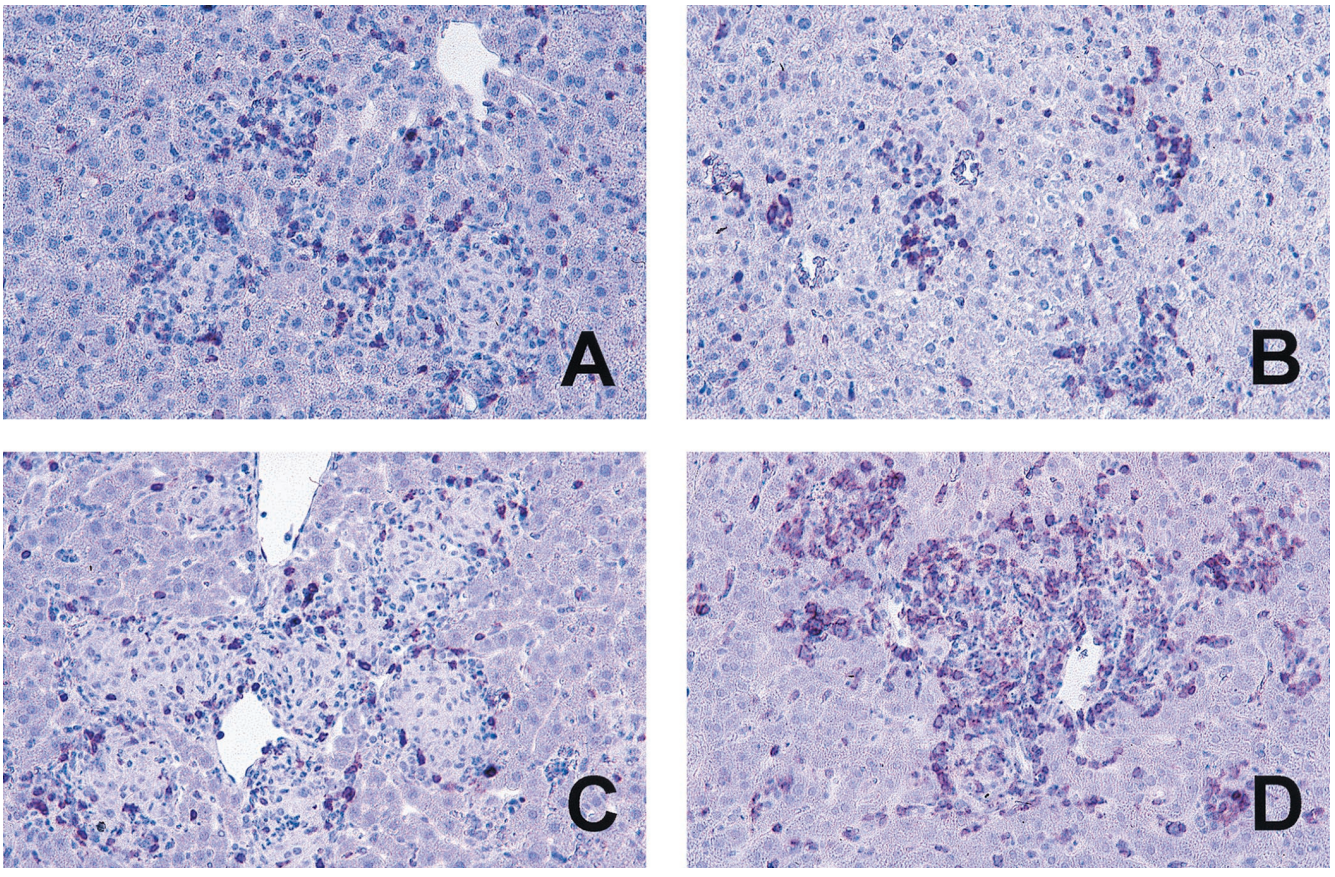

FIG. 6. $CD3^+$ cells in lesions of *M. avium*-infected $p55^{+/+}$ and $p55^{-/-}$ mice. Mice were intravenously infected with 10^6 CFU of *M. avium* TMC724 and sacrificed 3 weeks (A and B) or 5 weeks (C and D) after infection. Immunohistology was performed on paraffin-embedded liver sections with an anti-CD3 monoclonal antibody and peroxidase-linked secondary antibodies. (A and C) $p55^{+/+}$ mice; (B and D) $p55^{-/-}$ mice (×64).

weeks postinfection with TMC724 showed that, while IL-10 and IL-12 p40 mRNA levels in the liver were similar in $p55^{-/-}$ and immunocompetent mice, levels of mRNA for IFN-γ, TNF, and iNOS were significantly lower in $p55^{-/-}$ mice (twofold, fourfold, and fourfold decreases, respectively) (Fig. 7, columns A), reflecting the decreased number of infiltrating inflammatory cells in these mice at this early point of infection. Semiquantitative RT-PCR of liver tissue taken from TMC724-infected $p55^{-/-}$ mice 1 week prior to death, however, demonstrated that levels of mRNA for IFN-γ and IL-12 p40 (8-fold and 10-fold increases, respectively) were higher than in infected $p55^{+/+}$ mice, while IL-10, TNF, and iNOS mRNA levels were comparable to those found in immunocompetent mice (Fig. 7, columns B). IL-4 mRNA levels did not significantly differ from uninfected controls at any investigated point of infection. RT-PCR studies of SE01-infected mice gave similar results (data not shown). These findings were corroborated by ELISA measurements of cytokine protein levels, which also showed that in moribund $p55^{-/-}$ mice, IFN-γ and IL-12 levels were consistently higher in both spleen homogenates and plasma regardless of the *M. avium* isolate used for infection (Table 1). Plasma TNF levels of SE01-infected $p55^{-/-}$ mice at time of death were also significantly higher than in $p55^{+/+}$ mice (Table 1). Mice that were clinically worse always had the highest TNF and IFN-γ plasma levels. In agreement with RT-PCR results on iNOS expression, nitrite and nitrate levels (as an estimate of nitric oxide production) in the sera of *M. avium*-infected mice determined after 5 to 6 weeks of infection were similar, with levels slightly lower in $p55^{-/-}$ mice than in $p55^{+/+}$ mice (254 ± 95 μM versus 365 ± 39 μM, respectively). Taken together, these data show that there was a hyperinflammatory response with increased numbers of $CD3^+$ cells in the livers of *M. avium* infected $p55^{-/-}$ mice just prior to death and significantly higher amounts of IL-12 and IFN-γ present in tissue lesions.

DISCUSSION

The major finding from our studies is that, despite comparable *M. avium* counts in $p55^{+/+}$ and $p55^{-/-}$ mice, developing granulomas in $p55^{-/-}$ mice become necrotic and cause tissue damage. Granuloma necrosis in $p55^{-/-}$ mice is associated with increased infiltration of $CD3^+$ cells and higher IFN-γ and IL-12 tissue levels, and it is invariably followed by the death of all infected $p55^{-/-}$ mice, regardless of the virulence of the *M. avium* strain used for infection.

M. avium infection is known to progress in two phases in susceptible mice: after an initial phase of almost unrestrained growth with little inflammatory cell accumulation, $CD4^+$ T-cell-mediated effector mechanisms become apparent, resulting in granuloma formation (19) and growth reduction of strains of intermediate virulence (1). Our findings imply that TNFRp55 is not involved in antibacterial mechanisms operating during the early T-cell-independent and T-cell-dependent phases of infection. This interpretation is in agreement with a recent study showing that mice deficient for both components of

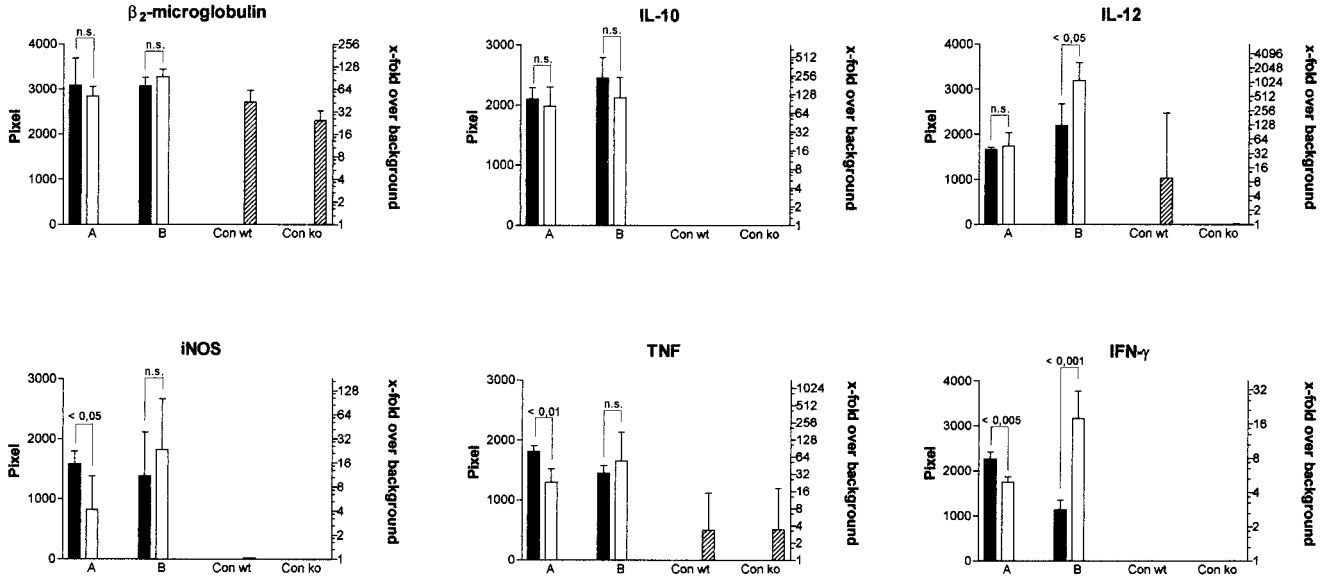

FIG. 7. Semiquantitative RT-PCR in the livers of $p55^{+/+}$ and $p55^{-/-}$ mice. RT-PCR with specific cytokine primers and hybridization with labelled internal probes were performed on liver samples taken at 3 weeks (columns A) or 5 weeks (columns B) after infection with TMC724. Mean pixel values of four individual mice ± SDs per experimental group are shown. Significant differences in pixel values between $p55^{+/+}$ mice (black columns) and $p55^{-/-}$ mice (white columns) are indicated. Crosshatched columns, uninfected controls; Con wt, $p55^{+/+}$ control; Con ko, $p55^{-/-}$ control. Twofold serial dilutions of positive control cDNA were included in each reaction to ascertain linear amplification rates and provide a scale of comparison for samples from different experimental groups. Background X-ray film exposure was arbitrarily set at a pixel value of 1, and calculated x-fold increases over background pixel values are shown on the right. *P* values used in statistical comparisons are indicated above pixel columns. n.s., not significantly different.

TNFR (p55 and p75) were similar to littermate controls in restricting the growth of an *M. avium* strain of intermediate virulence (10).

Since during the first 5 weeks of infection levels of *M. avium* growth were identical in the livers of $p55^{+/+}$ and $p55^{-/-}$ mice, we were in the position to assess the inflammatory response in infected livers uninfluenced by an exacerbation of infection known to occur in other experimental systems in these mice (e.g., during *M. tuberculosis* infection [17]). We found granuloma formation to be delayed in $p55^{-/-}$ mice compared to the formation rate in $p55^{+/+}$ mice. Granulomas in $p55^{-/-}$ mice had a more immature and malorganized appearance, but macrophages showed signs of activation, as evidenced by strong staining for iNOS protein. Signalling via TNFRp55 was previously shown not to be necessary for the expression and function of iNOS (14, 17), although we did find mRNA expression for iNOS to be delayed in $p55^{-/-}$ mice as a consequence of delayed mononuclear-cell recruitment (Fig. 7). In this context, it is important to remember that, in contrast to *M. tuberculosis*, most strains of *M. avium*, including the ones used here, are resistant to any direct antibacterial effects of nitric oxide (11).

These findings concerning the kinetics, quantity, and quality of granuloma formation reconcile a number of conflicting reports on the role of TNF during granuloma initiation (17, 25, 37, 38). Our kinetic investigations indicate that the speed and magnitude of granuloma formation and differentiation in the absence of TNFRp55 are determined by the virulence and inoculum size of the mycobacterium used. Therefore, when early points of infection are examined, little or no granuloma formation is evident in $p55^{-/-}$ mice whenever mycobacteria of

TABLE 1. Cytokine levels in spleen homogenates and plasma of $p55^{+/+}$ and $p55^{-/-}$ mice obtained 5 weeks postinfection

M. avium strain[b]	Test source (mouse tissue)	Level (pg/ml) of[a]:		
		TNF	IFN-γ	IL-12 p40
TMC724				
	Spleen homogenates ($p55^{+/+}$)	1,619 ± 254	812 ± 88	5,007 ± 179
	Spleen homogenates ($p55^{-/-}$)	1,524 ± 477	**2,655** ± 502**[c]	5,070 ± 115
	Plasma ($p55^{+/+}$)	3,512 ± 480	<50	7,343 ± 519
	Plasma ($p55^{-/-}$)	6,938 ± 5,261	**7,536** ± 2,740**	**12,087** ± 2,582*
SE01				
	Spleen homogenates ($p55^{+/+}$)	1,182 ± 178	370 ± 111	3,312 ± 267
	Spleen homogenates ($p55^{-/-}$)	1,274 ± 291	**1,342** ± 635*	**5,265** ± 1,524*
	Plasma ($p55^{+/+}$)	681 ± 83	<50	4,639 ± 308
	Plasma ($p55^{-/-}$)	**5,068** ± 1,804	**3,634** ± 1,404**	**7,806** ± 2,089*

[a] Values are the means of four to six mice per group (± SD). Boldface type indicates values for $p55^{-/-}$ mice significantly different from those for $p55^{+/+}$ mice.
[b] Cytokine levels for uninfected mice were as follows: TNF, 690 pg/ml (spleen homogenates) and 924 pg/ml (plasma); IFN-γ, 325 pg/ml (spleen homogenates) and <50 pg/ml (plasma); and IL-12 p40, 274 pg/ml (spleen homogenates) and 1,712 pg/ml (plasma).
[c] *, $P < 0.05$; **, $P < 0.005$.

low virulence, such as *M. bovis* BCG or *M. avium*, are used for infection (37). At later points of infection with these strain, or during infection with highly virulent *M. tuberculosis*, there is little difference in the granuloma number in $p55^{-/-}$ mice compared to the number in $p55^{+/+}$ mice, and epithelioid differentiation and macrophage activation does occur to a significant extent (17).

Flynn et al. also noted granuloma necrosis in $p55^{-/-}$ mice infected with *M. tuberculosis* (17). In those experiments, however, it was difficult to ascertain the cause of tissue destruction, because *M. tuberculosis* proliferated extensively due to the absence of TNF-mediated antimycobacterial effects. In that situation, macrophages of $p55^{-/-}$ mice rendered incapable of controlling growth of *M. tuberculosis* may have been lysed after reaching a threshold load, causing necrotic destruction of granulomatous and parenchymal tissue. In fact, an identical histopathology was described in *M. tuberculosis*-infected mice deficient for β2-microglobulin, the αβ-T-cell receptor, IFN-γ, or iNOS (7, 16, 28, 29), implying that unrestricted growth of *M. tuberculosis* is the common determining cause of tissue necrosis, rather than a specific effect due to the absence of TNFRp55.

In contrast, our experiments demonstrate that long-term macrophage integrity and granuloma maintenance during chronic *M. avium* infection are dependent on TNFRp55-mediated functions distinct from those known to induce antibacterial effector mechanisms. While both this function of regulating granuloma stability and the known antimycobacterial effects induced by TNF may be important in containing infection with *M. tuberculosis*, only the former is critical in determining the outcome of *M. avium* infection.

The view that $p55^{-/-}$ mice died not as a consequence of the exacerbation of mycobacterial proliferation or dissemination, but rather because of the pathology (i.e., necrosis) caused by granuloma disintegration, is supported by the fact that mice are capable of tolerating much higher numbers of *M. avium* than *M. tuberculosis* in infected organs. For instance, infection with *M. avium* TMC724 in immunocompetent mice leads to bacterial organ loads in excess of 10^{10} CFU and is accompanied by heavy dissemination into the kidneys and the brain without any apparent impairment of vital organ functions (12a, 19). Although during this scenario granuloma macrophages are completely filled with mycobacteria, we have never observed signs of cell death or granuloma necrosis resembling those in $p55^{-/-}$ mice, where they occur at a much lower mycobacterial load and even during infection with a strain of lower virulence.

Disintegration of the granulomatous lesion initially involved apoptosis of mononuclear cells followed by a necrotic decomposition of the entire granuloma structure. Hepatocyte necrosis with concomitantly increased levels of hepatic transaminases in serum ensued, and this might have constituted the direct cause of death in intravenously infected $p55^{-/-}$ mice. In view of the disproportionately increased levels of LDH, it is also possible that necrosis in tissues other than the liver (e.g., the lung) may have occurred. We have been unable to find histopathologic signs of granuloma necrosis in other organs after intravenous infection. However, in a study focusing on the long-term immunopathological sequelae of aerogenic exposure to *M. avium* in immunocompetent and -deficient mice, we observed that $p55^{-/-}$ mice died at approximately the same rate as their intravenously infected littermates yet showed few signs of hepatocyte necrosis, while they had necrotizing granulomatous infiltrations in the lungs (3). Therefore, granuloma breakdown, as such, rather than isolated hepatocyte necrosis, seems to be a prerequisite for the death of $p55^{-/-}$ mice resulting from *M. avium* infection. Granuloma necrosis was always followed by increased growth of *M. avium*, primarily in less-affected organs, such as the kidney and brain. This suggests dissemination of mycobacteria from disintegrating primary granulomas and substantiates the generally held belief that a major function of granulomas is to physically prevent bacterial spreading by isolating infectious foci.

Traditionally, TNF has been thought to act as a major inducer of tissue pathology, particularly in tuberculous lesions (9, 36). However, $p55^{-/-}$ mice infected with *Leishmania major* were previously found to have larger inflammatory lesions than $p55^{+/+}$ mice, although they remained fully capable of eliminating parasites from the lesions (39). Moreover, contact hypersensitivity reactions to dinitrofluorobenzene were enhanced in $p55^{-/-}$ mice compared to syngeneic $p55^{+/+}$ mice (27). In these situations, TNFRp55-mediated signalling would seem to be involved in restricting or resolving, rather than exacerbating, the inflammatory response.

It seems possible that TNF regulates the inflammatory response by maintaining the viability of activated macrophages at the site of infection. *M. avium* may have a direct or indirect toxic effect on macrophages, and TNFRp55-generated signals may be needed to antagonize any such effect. In this respect, in vitro cell culture systems demonstrated that mycobacterial infection may lead to macrophage apoptosis, particularly when high numbers of mycobacteria are used (35), and that TNF may, in part, counteract apoptosis, increasing the survival of infected macrophages (12, 30).

The concept of a regulatory role for TNF in chronic inflammation is further supported by results recently obtained in TNF gene-deficient mice experimentally challenged with heat-killed *C. parvum* (38). These mice also developed poorly organized hyperinflammatory lesions in their livers and spleens and showed disseminated foci of necrosis shortly before death (31). Evidence for an unbalanced, hyperinflammatory response in the absence of TNF signalling was also obtained in the present studies of persistent mycobacterial infection. When we examined the lesions in $p55^{-/-}$ mice by immunohistology, there was a threefold increase in tissue-infiltrating $CD3^+$ cells in the livers of infected $p55^{-/-}$ mice, and mRNA and protein levels for IFN-γ and IL-12 (and inconsistently for TNF) were significantly higher in the liver, spleen, and plasma of these $p55^{-/-}$ mice than in $p55^{+/+}$ mice. It is therefore possible that a disregulated T-cell-mediated and/or IFN-γ-dependent process led to granuloma necrosis.

It is unknown whether, during certain stages of granuloma development in human mycobacterial infections, expression of TNF or its receptors is down modulated. It is clear from histological studies that apoptosis and necrosis frequently occur in mycobacterial granulomas (8, 9, 23). In view of the evidence presented here, it seems possible that necrotic breakdown of tuberculous lesions may also be a consequence of a decrease, rather than an increase, in TNF signalling and of a concomitant disregulation of the T-cell response within the lesion.

ACKNOWLEDGMENTS

This work was supported in part by a grant from the Deutsche Forschungsgemeinschaft (Eh 101/4-1).

We acknowledge the excellent technical assistance of Claudia Hahn.

REFERENCES

1. **Appelberg, R., A. G. Castro, J. Pedrosa, R. A. Silva, I. M. Orme, and P. Minóprio.** 1994. Role of gamma interferon and tumor necrosis factor alpha during T-cell-independent and -dependent phases of *Mycobacterium avium* infection. Infect. Immun. **62:**3962–3971.
2. **Appelberg, R., A. Sarmento, and A. G. Castro.** 1995. Tumour necrosis factor alpha in the host resistance to mycobacteria of distinct virulence. Clin. Exp. Immunol. **101:**308–313.

3. **Benini, J., E. M. Ehlers, and S. Ehlers.** Different types of pulmonary grnuloma necrosis in immunocompetent vs. TNFRp55-gene-deficient mice aerogenically infected with highly virulent *Mycobacterium avium*. J. Pathol., in press.
4. **Blake, J. A., J. T. Eppig, J. E. Richardson, M. T. Davisson, and the Mouse Genome Informatics Group.** 1998. The mouse genome database (MGD)—a community resource. Status and enhancement. Nucleic Acids Res. **26:**130–137.
5. **Cattoretti, G., S. Piteri, C. Parraricini, M. A. G. Becker, S. Poggi, C. Bifulco, G. Key, L. D'Amato, E. Sabattini, E. Fendale, F. Geynolds, J. Gerdes, and F. Rilke.** 1993. Antigen unmasking on formalin-fixed, paraffin-embedded tissue sections. J. Pathol. **171:**83–98.
6. **Collins, F. M., and R. W. Stokes.** 1987. *Mycobacterium avium* complex infections in normal and immunodeficient mice. Tubercle **68:**127–136.
7. **Cooper, A. M., D. K. Dalton, T. A. Stewart, J. P. Griffin, D. G. Russell, and I. M. Orme.** 1993. Disseminated tuberculosis in interferon γ gene-disrupted mice. J. Exp. Med. **178:**2243–2248.
8. **Cree, I. A., S. Nurbhai, G. Milne, and J. S. Beck.** 1987. Cell death in granulomata: the role of apoptosis. J. Clin. Pathol. **40:**1314–1319.
9. **Dannenberg, A. M., and G. A. W. Rook.** 1994. Pathogenesis of pulmonary tuberculosis: an interplay of tissue-damaging and macrophage-activating immune responses, p. 459–483. *In* B. R. Bloom (ed.), Tuberculosis—pathogenesis, protection, and control. ASM Press, Washington, D.C.
10. **Doherty, T. M., and A. Sher.** 1997. Defects in cell-mediated immunity affect chronic, but not innate, resistance of mice to *Mycobacterium avium* infection. J. Immunol. **158:**4822–4831.
11. **Doi, T., M. Ando, T. Akaike, M. Suga, K. Sato, and H. Maeda.** 1993. Resistance to nitric oxide in *Mycobacterium avium* complex and its implication in pathogenesis. Infect. Immun. **61:**1980–1989.
12. **Dürrbaum-Landmann, I., J. Gercken, H.-D. Flad, and M. Ernst.** 1996. Effect of in vitro infection of human monocytes with low numbers of *Mycobacterium tuberculosis* bacteria on monocyte apoptosis. Infect. Immun. **64:**5384–5389.

12a. **Ehlers, S.** Unpublished observations.

13. **Ehlers, S., and U. Seitzer.** 1998. Measuring immune responses in vivo, p. 365–387. *In* S. Kaufmann and D. Kabelitz (ed.), Methods in microbiology, vol. 25. Immunology of infection. Academic Press, London, United Kingdom.
14. **Endres, R., A. Luz, H. Schulze, H. Neubauer, A. Futterer, S. M. Holland, H. Wagner, and K. Pfeffer.** 1997. Listeriosis in p47(phox−/−) and Trp55−/− mice: protection despite absence of ROI and susceptibility despite presence of RNI. Immunity **7:**419–432.
15. **Flesch, I. E., and S. H. E. Kaufmann.** 1993. Role of cytokines in tuberculosis. Immunobiology **189:**316–339.
16. **Flynn, J. L., M. M. Goldstein, K. J. Triebold, B. Koller, and B. R. Bloom.** 1992. Major histocompatibility complex class I-restricted T cells are required for resistance to *Mycobacterium tuberculosis* infection. Proc. Natl. Acad. Sci. USA **89:**12013–12017.
17. **Flynn, J. L., M. M. Goldstein, J. Chan, K. J. Triebold, K. Pfeffer, C. J. Lowenstein, R. Schreiber, T. W. Mak, and B. R. Bloom.** 1995. Tumor necrosis factor-α is required in the protective immune response against *Mycobacterium tuberculosis* in mice. Immunity **2:**561–572.
18. **Garcia, I., Y. Miyazaki, G. Marchal, W. Lesslauer, and P. Vassalli.** 1997. High sensitivity of transgenic mice expressing soluble TNFR1 fusion protein to mycobacterial infections: synergistic action of TNF and IFN-gamma in the differentiation of protective granulomas. Eur. J. Immunol. **27:**3182–3190.
19. **Hänsch, H. C. R., D. A. Smith, M. E. A. Mielke, H. Hahn, G. J. Bancroft, and S. Ehlers.** 1996. Mechanisms of granuloma formation in murine *Mycobacterium avium* infection: the contribution of CD4+ T cells. Int. Immunol. **8:**1299–1310.
20. **Horsburgh, C. R., J. A. Haavlik, D. A. Ellis, E. Kennedy, S. A. Fann, R. E. Dubois, and S. E. Thompson.** 1991. Survival of patients with AIDS and disseminated *Mycobacterium avium* complex infection with and without antimycobacterial chemotherapy. Am. Rev. Respir. Dis. **144:**557–559.
21. **Inderlied, C. B., C. A. Kemper, and L. E. Bermudez.** 1993. The *Mycobacterium avium* complex. Clin. Microbiol. Rev. **6:**266–310.
22. **Jacobson, M. A., P. C. Hopewell, D. M. Yajko, W. K. Hadley, E. Lazarus, P. K. Mhanty, G. W. Modin, D. W. Feigal, P. S. Cusick, and M. A. Sande.** 1991. Natural history of disseminated *Mycobacterium avium* complex infection in AIDS. J. Infect. Dis. **164:**994–998.
23. **Jagirdar, J., and D. Zagzag.** 1996. Pathology and insights into pathogenesis of tuberculosis, p. 467–482. *In* W. N. Rom and S. Garay (ed.), Tuberculosis. Little, Brown and Co., Boston, Mass.
24. **Kaufmann, S. H. E.** 1993. Immunity to intracellular bacteria. Annu. Rev. Immunol. **11:**129–163.
25. **Kindler, V., A.-P. Sappino, G. E. Grau, P.-F. Piguet, and P. Vassalli.** 1989. The inducing role of tumor necrosis factor in the development of bactericidal granulomas during BCG infection. Cell **56:**731–740.
26. **Klatt, E. C., D. F. Jensen, and P. R. Meyer.** 1987. Pathology of *Mycobacterium avium intracellulare* infection in acquired immunodeficiency syndrome. Hum. Pathol. **18:**709–714.
27. **Kondo, S., B. Wang, H. Fujisawa, G. M. Shivji, B. Echtenacher, T. W. Mak, and D. N. Sauder.** 1995. Effect of gene-targeted mutation in TNF receptor (p55) on contact hypersensitivity and ultraviolet B-induced immunosuppression. J. Immunol. **155:**3801–3805.
28. **Ladel, C. H., C. Blum, A. Dreher, K. Reifenberg, and S. H. E. Kaufmann.** 1995. Protective role of γδ T cells and αβ T cells in tuberculosis. Eur. J. Immunol. **25:**2877–2881.
29. **MacMicking, J., R. North, R. LaCourse, J. Mudgett, S. Shah, and C. F. Nathan.** 1997. Identification of NOS2 as a protective locus against tuberculosis. Proc. Natl. Acad. Sci. USA **94:**5243–5248.
30. **Mangan, D. F., G. R. Welch, and S. M. Wahl.** 1991. Lipopolysaccharide, tumor necrosis factor-α, and IL-1β prevent programmed cell death (apoptosis) in human peripheral blood monocytes. J. Immunol. **146:**1541–1546.
31. **Marino, M. W., A. Dunn, D. Grail, M. Inglese, Y. Noguche, E. Richards, A. Jungbluth, H. Wada, M. Moore, B. Williamson, S. Basu, and L. J. Old.** 1997. Characterization of tumor necrosis factor-deficient mice. Proc. Natl. Acad. Sci. USA **94:**8093–8098.
32. **Mouse Genome Database.** 1996, copyright date. [Online.] Mouse genome informatics. The Jackson Laboratory, Bar Harbor, Maine. http://www.informatics.jax.org/ [2 March 1999, last date accessed.]
33. **Pedrosa, J., M. Florido, Z. M. Kunze, A. G. Castro, F. Portaels, J. McFadden, M. T. Silva, and R. Appelberg.** 1994. Characterization of the virulence of *Mycobacterium avium* complex (MAC) isolates in mice. Clin. Exp. Immunol. **98:**210–216.
34. **Pfeffer, K., T. Matsuyama, T. M. Kundig, A. Wakeham, K. Kishihara, A. Ahahinian, K. Wiegmann, P. S. Ohashi, M. Krönke, and T. W. Mak.** 1993. Mice deficient for the 55kd tumor necrosis factor receptor are resistant to endotoxic shock, yet succumb to *L. monocytogenes* infection. Cell **73:**457–467.
35. **Placido, R., G. Mancino, A. Amendola, F. Mariani, S. Vendetti, M. Piacentini, A. Sanduzzi, M. L. Bocchino, M. Zembala, and V. Colizzi.** 1997. Apoptosis of human monocytes/macrophages in *Mycobacterium tuberculosis* infection. J. Pathol. **181:**31–38.
36. **Rook, G. A. W., and B. R. Bloom.** 1994. Mechanisms of pathogenesis of tuberculosis, p. 485–501. *In* B. R. Bloom (ed.), Tuberculosis—pathogenesis, protection, and control. ASM Press, Washington, D.C.
37. **Senaldi, G., S. Yin, C. L. Shaklee, P.-F. Piguet, T. W. Mak, and T. R. Ulich.** 1996. *Corynebacterium parvum*- and *Mycobacterium bovis* Bacillus Calmette-Guerin-induced granuloma formation is inhibited in TNF receptor I (TNF-RI) knockout mice and by treatment with soluble TNF-RI. J. Immunol. **157:**5022–5026.
38. **Smith, D. A., H. C. R. Hänsch, G. J. Bancroft, and S. Ehlers.** 1997. T cell independent granuloma formation in response to *Mycobacterium avium*—role of tumour necrosis factor-α and interferon-γ. Immunology **92:**413–421.
39. **Vieira, L. Q., M. Goldschmidt, M. Nashleanas, K. Pfeffer, T. Mak, and P. Scott.** 1996. Mice lacking the TNF receptor p55 fail to resolve lesions caused by infection with *Leishmania major*, but control parasite replication. J. Immunol. **157:**827–835.

Editor: S. H. E. Kaufmann